Title

Deep Optic Nerve Head Structures Associated With Increasing Axial Length in Healthy Myopic Eyes of Moderate Axial Length.

Authors

Saito, Hitomi

Kambayashi, Mitsuki

Araie, Makoto

et al.

Publication Date

2023-05-01

DOI

10.1016/j.ajo.2023.01.003

Peer reviewed

HHS Public Access

Author manuscript

Am J Ophthalmol. Author manuscript; available in PMC 2024 May 01.

Published in final edited form as:

Am J Ophthalmol. 2023 May ; 249: 156–166. doi:10.1016/j.ajo.2023.01.003.

Deep Optic Nerve Head Structures Associated With Increasing Axial Length in Healthy Myopic Eyes of Moderate Axial Length

HITOMI SAITO,

MITSUKI KAMBAYASHI,

MAKOTO ARAIE,

HIROSHI MURATA,

NOBUKO ENOMOTO,

TSUTOMU KIKAWA,

KAZUHISA SUGIYAMA,

TOMOMI HIGASHIDE,

ATSUYA MIKI,

AIKO IWASE,

GOJI TOMITA,

TORU NAKAZAWA,

MAKOTO AIHARA,

KYOKO OHNO-MATSUI,

TAE-WOO KIM,

CHRISTOPHER KAI SHUN LEUNG,

LINDA M. ZANGWILL,

ROBERT N. WEINREB

Department of Ophthalmology, Graduate School of Medicine, University of Tokyo (H.S., M.K., M.Ai.), Tokyo, Japan; Kanto Central Hospital of the Mutual Aid Association of Public School Teachers (M.Ar.), Tokyo, Japan; Center Hospital of the National Center for Global Health and Medicine (H.M.), Tokyo, Japan; Japan Community Health care Organization Tokyo Shinjuku Medical Center (N.E.), Tokyo, Japan; R&D Division, Topcon Corporation (T.K.), Tokyo, Japan; Department of Ophthalmology, Kanazawa University Graduate School of Medical Sciences (K.S., T.H.), Kanazawa, Japan; Department of Innovative Visual Science, Osaka University Graduate School of Medicine (A.M.), Osaka, Japan; Department of Myopia Control Research, Aichi Medical University Medical School (A.M.), Nagakute, Japan; Tajimi Iwase Eye Clinic (A.I.), Tajimi, Japan; Department of Ophthalmology, Toho University Ohashi Medical Center (G.T.), Tokyo, Japan; Department of Ophthalmology, Graduate School of Medicine, Tohoku University (T.N.), Sendai, Japan; Department of Ophthalmology and Visual Science, Tokyo Medical and Dental University (K.O.-M.), Tokyo, Japan; Department of Ophthalmology, Seoul National University College of Medicine, Seoul National University Bundang Hospital (T.-W.K.), Seongnam, Korea; Department

Inquiries to Hitomi Saito, Department of Ophthalmology, Graduate School of Medicine, University of Tokyo, Tokyo, Japan; hitomi8678@gmail.com.

of Ophthalmology, LKS Faculty of Medicine, University of Hong Kong (C.K.S.L.), Hong Kong Special Administrative Region, China; Hamilton Glaucoma Center, Shiley Eye Institute (L.M.Z., R.N.W.), and the Viterbi Family Department of Ophthalmology (L.M.Z., R.N.W.), University of California San Diego, La Jolla, California, USA.

Abstract

PURPOSE: To elucidate which swept-source optical coherence tomography (OCT)–derived optic nerve head (ONH) parameters are associated with longer axial length (AXL) in healthy myopic eyes.

DESIGN: Prospective cross-sectional observational study.

METHODS: Two hundred eleven healthy eyes of 140 participants (96 emmetropic-mild myopic [AXL: 22.2–24.5 mm], 83 moderately myopic [24.5–26.0 mm], and 32 highly myopic [26.0–27.4 mm] eyes) were enrolled. Bruch membrane opening (BMO), anterior scleral canal opening (ASCO) area and ovality, minimum rim width, parameters defining misalignment between the BMO and ASCO planes, OCT-defined region of perineural canal retinal epithelium atrophy and externally oblique choroidal border tissue, circumpapillary retinal nerve fiber layer thickness (cpRNFLT), circumpapillary choroidal thickness (cpChT), lamina cribrosa parameters, and peripapillary scleral (PPS) angle were calculated from BMO-centered radial scans reconstructed from 3D raster scans. Multivariate linear mixed models were used to elucidate ONH parameters that are independently associated with AXL.

RESULTS: Longer AXL was associated with a greater misalignment between ASCO and BMO planes, larger region of externally oblique choroidal border tissue, thinner cpChT, larger PPS angle, larger ASCO area, and thicker cpRNFLT (all $P < .040$ after Bonferroni's correction for number of included explanatory variables).

CONCLUSIONS: A greater misalignment between BMO and ASCO planes, thinner choroid, a more posteriorly bowed PPS, an enlargement of ASCO, and thicker cpRNFLT were each associated with longer AXL. An enhanced understanding of these AXL-associated configurations should provide essential information to improve our ability to detect glaucoma-induced ONH morphology in myopic eyes.

The global prevalence of myopia is increasing rapidly, [1] and myopia is an important risk factor for many ophthalmologic diseases, [2] including glaucoma. [3] Myopic optic nerve heads (ONHs) are well known to accompany characteristic structure changes. Compared with a nonmyopic ONH, a myopic ONH typically has a larger disc area, more oval shape, greater tilt, enlarged peripapillary atrophy (PPA), and a shallower optic cup. [4–10] These structural changes are observed in both high and pathologic myopia, as well as in mild to moderate non-pathologic myopia. Furthermore, structural changes caused by myopia often mimic glaucomatous changes and confound diagnosis of glaucomatous optic neuropathy in myopic eyes.[11–13] As the prevalence of myopia is high in Eastern Asian countries, [14, 15] distinguishing between healthy and glaucomatous ONHs in these eyes can often be challenging.[16]

Recently, technological advances of optical coherence tomography (OCT) have facilitated visualization of the deeper structures of the ONH. One type of this new technology is the swept-source OCT (SS-OCT). SS-OCT uses a short cavity swept laser with a center wavelength of 1050 nm and a sweeping range of approximately 100 nm, enabling deeper light penetration with less variability in sensitivity with depth. [17] With SS-OCT, there is improved visibility of the outer layers of the eye, including the choroid, sclera, and lamina cribrosa (LC), compared with conventional SD-OCT images even with the use of enhanced depth imaging mode. [18–20]

Several reports have investigated the relationship of myopic refractive error and/or axial length (AXL) with individual ONH parameters measured from OCT images in healthy myopic eyes. [8–10, 21–26] Myopic ONH structural changes that may be associated with connective tissue remodeling is more directly influenced by myopic AXL elongations. [2, 27] Furthermore, most of these ONH parameters are well correlated with each other, and it is unclear which ONH parameters are independently associated with longer AXL. Hence, a comprehensive study based on AXL adjusting for these interparameter correlations is needed for an improved understanding of the relationship between AXL and ONH morphology in healthy myopic eyes. The purpose of this study is to investigate which of all the measurable SS-OCT–derived ONH parameters in healthy myopic eyes are fundamentally associated with longer AXL after considering interparameter correlations.

METHODS

PARTICIPANTS:

Emmetropic and myopic healthy participants were separately recruited for this prospective cross-sectional observational study, using identical inclusion criteria from 8 institutions (Kanazawa University, Osaka University, Tajimi Iwase Eye Clinic, Toho University Ohashi Medical Center, Tohoku University, Seoul National University Bundang Hospital, University of California San Diego, and University of Hong Kong). Study protocols were approved by the institutional review board of Kanto Central Hospital (R1–06-005) and adhered to the tenets of the Declaration of Helsinki. All patients provided written informed consent before participation to the study.

Self-reported 30- to 70 -year-old healthy volunteers were included as healthy participants. Ocular examinations, including refraction and corneal radius of curvature measurements (ARK-900; NIDEK), best-corrected visual acuity (BCVA) measurements with the 5-m Landolt chart, AXL measurements (IOL Master; Carl Zeiss Meditec, Inc), slitlamp examination, intraocular pressure (IOP) measurements with Goldmann applanation tonometry, dilated funduscopy, fundus photography, stereophotography. and visual field testing with myopia correction using Humphrey field analyzer (HFA) 24–2 Swedish Interactive Threshold Algorithm Standard program (Carl Zeiss Meditec, Inc) were performed at the first visit.

Inclusion criteria for this study were (1) nonglaucomatous optic disc appearance based on detailed stereophotograph observation (by M.Ar., A.I., G.T., K.O.M.); (2) spherical equivalence (SE) ≤+ 1 diopter (D), astigmatism < 2 D; (3) IOP ≤21 mm Hg; (4) BCVA >

20/25; (5) AXL < 28 mm; and (6) attainment of good quality of SS-OCT images and fundus photographs.

Exclusion criteria were contraindications to pupillary dilation, narrow angle (Shaffer grade ≤ 2), abnormal HFA results following criteria defined by the Hodapp-Parrish-Anderson criteria, [28] unreliable HFA results (fixation loss or false negative > 20%, false positive > 15%), history of intraocular or refractive surgery, family history of glaucoma, history of ocular or systemic diseases that could affect results of HFA or OCT examinations (ie, glaucoma, clinically significant cataract, diabetic retinopathy and/or maculopathy, age-related macular degeneration, epiretinal membrane), optic nerve or retinal abnormality, history of systemic steroid or anticancer drugs, and clinically significant hyper- or hypotension.

Pathologically myopic eyes or its suspects (ie, eyes with optic disc ovality > 1.33 on fundus photography observation, [29] inverted optic discs, posterior staphyloma, focal and/or diffuse macular chorioretinal atrophy, intrachoroidal cavitation, and circular PPA zones) were excluded by a specialist in the field (K.O.M.). If one eye of a participant met the exclusion criteria, both eyes were excluded from the study.

OCT MEASUREMENTS:

After pupillary dilation, the ONH and macula of all participants were imaged by SS-OCT (DRI OCT Triton; Topcon, Inc). Refractive correction, keratometry values, and AXL were specified before acquisition of data to correct for magnification effects on fundus image size, including the scan circle size on which circumpapillary retinal nerve fiber layer thickness (cpRNFLT) and circumpapillary choroidal thickness (cpChT) were measured. Corrections were made using a modified Littmann equation [30] provided by the manufacturer that is based on refractive error, corneal radius, and AXL.

For each participant, 6.0 × 6.0-mm raster scans centered on the optic disc, 24-line Bruch membrane opening (BMO)–centered radial scans (BMO was manually identified in 2 perpendicular ONH radial scans prior to acquisition to determine BMO center), and 12.0 × 9.0-mm-wide scans including both the ONH and macula were obtained. Measurements were repeated 3 times and data with the best quality factor were used. Images influenced by involuntary blinking or saccade or those with a quality factor < 60% were excluded.

Raw OCT data were exported from the device and imported into an original software developed for this study. Eight BMO points were identified on 4 scans to determine the BMO center on the raster scan. Circumpapillary retinal nerve fiber layer thickness (cpRNFLT) and circumpapillary choroidal thickness (cpChT) were measured along a 3.4-mm BMO-centered diameter annulus. All scans were checked and corrected for cpRNFLT and cpChT segmentation errors by 3 experienced examiners (H.S., M.K., T.K.).

Twelve BMO-centered radial scans were reconstructed from the raster scan for final segmentation. The fovea was manually determined on the wide scans and were registered with the raster scans to calculate the fovea-BMO (Fo-BMO) center axis. The retinal pigment epithelium (RPE) edge, BMO, and anterior scleral canal opening (ASCO) (determined as

the point where the projection of the anterior scleral surface intersects with the neural canal) were manually determined on both sides of the 12 BMO-centered radial scans reconstructed from the raster scans by 2 experienced examiners (H.S., M.K.) (Figure 1).

The 24-line radial ONH scans (and not the reconstructed radial scans) were used as a reference to confirm the manually determined segmentation when necessary (Supplemental Figure S1). When there was segmentation disagreement between the 2 examiners, a third examiner (M.Ar.) arbitrated the decisions. Intraobserver (H.S.) and interobserver (H.S. and K.M.) repeatability for RPE-, BMO-, and ASCO-related parameter measurements were calculated on 30 randomly selected participants. Reexaminations were performed on separate days with examiners masked to previous results.

The clinical disc margin was manually delineated on the infrared images of the raster scans. Disc area, disc ovality (the ratio of the long and short axes), and disc torsion (angle between the long axis of the optic disc and a line perpendicular to the Fo-BMO axis, with a positive torsion angle signifying an inferotemporal torsion) [31] were calculated for analysis.

ONH parameters including the area and ovality of the BMO and ASCO, and minimum rim width (MRW) were calculated from the obtained segmentation information. ASCO-BMO plane misalignment parameters were adapted from the definition described by Hong and associates. [22] Magnification effects of area and magnitude parameters were also corrected according to the manufacturer's formula as mentioned before.

ASCO-BMO offset magnitude (representing the magnitude of ASCO plane misalignment in reference to the BMO plane) was defined as the distance between the BMO centroid and ASCO centroid projected onto the BMO plane (Figure 2).[22] ASCO-BMO offset direction (representing the direction of misalignment of the ASCO plane in reference to the BMO plane) was defined as the angle between the Fo-BMO axis and the vector connecting the BMO centroid and ASCO centroid projected onto the BMO plane [22] (Figure 2).

The region of perineural canal RPE atrophy (clinically referred to as the PPA region with RPE atrophy, beta-zone PPA, [9, 32, 33] or βPPA + BM [6, 8, 34, 35]) was defined as the area between the RPE edge and BMO contour. The region of externally oblique choroidal border tissue configuration (clinically referred to as the PPA region without BM, gamma-zone PPA, [7, 9, 32, 33] or βPPA-BM [6, 8, 34, 35]) was defined as the area between the BMO contour and ASCO contour.

LC and peripapillary scleral (PPS) measurements were made using commercial artificial intelligence software, Reflectivity (Abyss Processing). [36, 37] The software automatically delineated the Bruch membrane, anterior LC surface, and peripapillary anterior scleral surface after enhancing visibility of the OCT raster scan by removing noises, shadows, and artifacts. In regions where there was not enough information for automatic delineation, the segmentations were left blank. Segmentation errors were checked by 2 experienced ophthalmologists (H.S., N.E.), and eyes with Bruch membrane, anterior LC surface, or peripapillary anterior scleral surface segmentation errors and/or invisibility were excluded from the study.

LC depth was defined as the distance between the BMO plane and anterior LC surface at the BMO center. The LC global shape index (LC-GSI) is an index with a numerical value between –1 and 1 that quantifies the global shape of the LC anterior boundary calculated from the maximum and minimum principal arc curvatures of the anterior LC surface. [36] The PPS angle quantifies the amount of PPS bowing and is defined as the angle between 2 lines parallel to the anterior scleral boundaries on a single horizontal B-scan in the nasal-temporal direction (Figure 3). A larger angle represents a more posteriorly bowed V-shaped PPS configuration.[37,38]

STATISTICAL ANALYSIS:

All statistical analyses were performed with IBM SPSS statistics (version 27; International Business Machines Corp). Pearson correlation tests were used for univariate correlation analysis in a sub dataset of 140 eyes of 140 participants to avoid intereye correlation. Intra- and interobserver repeatability of the RPE-, BMO-, and ASCO-related parameters were calculated by intraclass correlation coefficients using a 2-way mixed model for agreement.

Multivariate linear mixed models taking intereye correlations into account with AXL as the response variable were used to determine explanatory variables independently associated with longer AXL. The considered explanatory variables were age, BMO area, BMO ovality, ASCO area, ASCO ovality, ASCO-BMO offset magnitude, ASCO-BMO offset direction, area of region of perineural canal RPE atrophy, area of region of externally oblique choroidal border tissue configuration, MRW, cpRNFLT, cpChT, LC depth, LC-GSI, and PPS angle. Mixed linear models of all possible combinations of these 15 parameters (2^{15} – 1 combinations in all) were generated, and the model with the best fit (lowest Akaike information criterion) was selected for discussion.

Because both ASCO-BMO offset magnitude and the region of externally oblique choroidal border tissue configuration are parameters quantifying the misalignment of BMO and ASCO planes, they are strongly correlated with each other ($R = 0.800$, $P < .0001$; Supplemental Table 1). We created 2 models with region of externally oblique choroidal border tissue configuration excluded from the model when the ASCO-BMO offset magnitude was included and vice versa to avoid multicollinearity.[39] Bonferroni correction by the number of included explanatory variables in the best-fit model were conducted to account for multiple comparisons.

RESULTS

Data of 230 eyes of 155 healthy participants were collected. After excluding 19 eyes because of LC and scleral segmentation errors, 211 eyes of 140 participants that met the inclusion criteria were enrolled in the study. Baseline characteristics and results of the SS-OCT–derived ONH parameters of the healthy participants are presented in Table 1.

All RPE-, BMO-, and ASCO-related parameters showed good to excellent reproducibility, with intraclass correlation coefficients ranging from 0.889 (region of perineural canal RPE atrophy) to 0.988 (BMO area) for intraobserver reproducibility and 0.809 (ASCO-BMO offset direction) to 0.972 (BMO area) for interobserver reproducibility.

Univariate correlation analysis revealed that multiple ONH parameters were correlated with each other as well as with age and AXL, indicating the necessity to correct for these intercorrelations (all $P < .005$) (Supplemental Table 1).

The best-fit model including ASCO-BMO offset magnitude (but excluding the region of externally oblique choroidal border tissue configuration) indicated that longer AXL was significantly associated with larger ASCO-BMO offset magnitude, thinner cpChT, larger PPS angle, and thicker cpRNFLT (Table 2). The best-fit model that includes the region of externally oblique choroidal border tissue configuration (but excludes the ASCO-BMO offset magnitude) demonstrated similar results except that the ASCO area was significantly associated with longer AXL whereas the PPS angle was not selected in the model (Table 2).

Identical results were obtained when best-fit models were generated with optic disc parameters (disc area,[4] disc ovality,[5] and disc torsion,[31] which are reported to be associated with myopia or as risk factors for progression of myopic normal-tension glaucomatous eyes) additionally included as explanatory variables (Supplemental Table 2). ASCO-BMO offset magnitude and region of externally oblique choroidal border tissue configuration demonstrated the strongest association with AXL within each model, and a scattergram of the distribution of ASCO-BMO offset magnitude and AXL is presented in Figure 4.

DISCUSSION

Our results from the 2 best-fit models found that larger ASCO-BMO offset magnitude and region of externally oblique choroidal border tissue configuration had the strongest associations with AXL, suggesting that a greater misalignment of the BMO and ASCO planes leading to a region of externally oblique choroidal border tissues was the structural change most strongly associated with the degree of myopia in healthy myopic eyes. The mean ASCO-BMO offset direction was 162.8°±45.1°, indicating an inferior temporal misalignment of the BMO plane in reference to the ASCO plane. However, the direction itself did not demonstrate a significant association with AXL.

Recently, a study on mainly emmetropic Caucasian eyes revealed that the ASCO-BMO offset magnitude was positively associated with AXL.[22] The same investigators also reported that this magnitude was even larger in highly myopic healthy and glaucomatous eyes (AXL > 26.5 mm),[25] suggesting the role of ASCO-BMO plane misalignment in myopia. Our study attempted to further elucidate the nature of relationship of this misalignment, other ONH morphologic parameters, and AXL in an analysis including other peripapillary structural changes accompanying myopic AXL elongation such as area of region of perineural canal RPE atrophy, area of region of externally oblique choroidal border tissue configuration, choroidal thickness, LC, and peripapillary scleral configuration in healthy myopic eyes.

Our results were in accordance with the reports by Hong and associates finding greater ASCO-BMO offset magnitude to be associated with longer AXL.[22] This temporal shift of the BMO plane in myopic eyes also has been reported in histologic reports and on longitudinal observation in young children developing myopia.[7, 32]

Because the region of externally oblique choroidal border tissue configuration (clinically referred to as gamma-zone PPA or βPPA-BM) is defined as the region between the BMO and temporal ASCO margin, it can be thought of as representing the presence and degree of misalignment between BMO and ASCO planes. This is in accordance with histologic findings that suggest βPPA-BM results from stretching of the PPS that accompanies AXL elongation in myopic eyes.[7]

It has been generally assumed that the association of AXL is stronger with βPPA-BM[6-9] and that the region of perineural canal RPE atrophy (clinically referred to as beta-zone PPA or βPPA BM) is more strongly associated with aging and glaucomatous changes.[6, 33] However, reports on the characteristics of each type of PPA have been varied, and the precise relationship between PPA subtypes and myopia remains to be elucidated. βPPA BM and βPPA-BM width were both reported to be correlated with AXL in 74 moderately myopic (SE <–2 D)[9] and 80 highly myopic (AXL > 26 mm)[34] healthy eyes.

Dai and associates[33] also reported similar results on a wider range of AXL in 80 healthy eyes (21.9–33.6 mm). A longitudinal study on 23 myopic children by Lee and associates[35] reported that AXL elongation was mostly associated with the development of βPPA-BM, although significant concomitant development of βPPA BM was observed. Meanwhile, Kim and associates suggested that only βPPA-BM width is associated with AXL whereas βPPA BM may be an age-related atrophic change in 161 glaucomatous eyes.[6]

Our current study revealed that when adjustments for all measurable ONH parameters are taken into consideration, only the region of externally oblique choroidal border tissue configuration (βPPA-BM) area but not the region of perineural canal RPE atrophy (βPPA BM) area is positively associated with longer AXL ($P < .001$), and that this inferior temporal misalignment of the BMO plane quantified by the ASCO-BMO offset magnitude is the most important deep ONH change associated with longer AXL in healthy myopic eyes.

Our average ASCO-BMO offset magnitude (236.8±158.9 μm) was much larger in comparison to Hong and associates' report of 89.01±63.15 μm.[22] Values were most likely larger in our cohort because our average AXL was longer. (23.7 vs 24.82 mm) Although our ASCO-BMO offset magnitude was smaller than that of Jeoung and associates' cohort of mainly Caucasian highly myopic eyes with an average AXL of 26.96 mm (264.3±131.1 μm),[25] our values were very close to theirs despite the eyes in our cohort being much less myopic. This may be explained by some racial differences that Hong and associates reported. Asian eyes (n=22) in their cohort tended to have larger ASCO-BMO offset magnitude even after correction for AXL.[22] In addition, the ASCO-BMO offset values may vary because different OCT scans were used to measure the ASCO-BMO offset by Hong and associatesy[22] (Spectralis optic nerve head radial circle scans) than that used in the current study.

Correlation between longer AXL and thinner circumpapillary choroid has been reported from previous studies investigating the relationship between AXL and individual ONH parameters.[23] Thinning of the choroid is of special interest because it is also affected in glaucomatous eyes, and its associations with glaucomatous progression has been

suggested.[40] However, a recent study on glaucomatous eyes reported that thinner cpChT was only associated with longer AXL but not with glaucomatous visual field indices, suggesting that choroidal thinning is a myopic characteristic more than a glaucoma-related finding.[41] In accordance with previous studies, our study indicated that thinner choroid is associated with longer AXL even after taking other confounding ONH parameters into consideration.

Our study revealed that AXL is also associated with a larger PPS angle, which represents a more posteriorly bowed V-shaped PPS. This V-shaped PPS configuration has been reported to become more pronounced with older age,[37, 42] thinner choroidal thickness,[42] and in glaucomatous eyes when compared to healthy eyes.[38] A weak association between the PPS angle and AXL in univariate analysis but not in multivariate analysis taking age and cpChT into consideration was reported by Tun and associates in a cohort of middle-aged to elderly healthy participants.[37] We confirmed and expanded on their results by evaluating the effect of AXL on PPS structure on a cohort with a wider range of age and AXL including highly myopic eyes to demonstrate that posterior PPS bowing was independently associated with longer AXL after taking age and cpChT into consideration.

Larger ASCO area was also suggested to be associated with longer AXL. Our average ASCO area (2.82±0.58 mm2) was larger than that of both the mostly emmetropic and highly myopic cohort of mainly Caucasian eyes reported by Hong and associates[22] and Jeoung and associates[25] (2.22 and 2.26 mm^2, respectively). Because BMO area has been reported to be larger in Asian eyes when compared to European and African descent eyes,[10, 43] similar racial differences may be observed in ASCO area. Furthermore, the nasal ASCO was often difficult to determine in eyes with tilted discs because of limits in visibility, and there remains a possibility that the nasal ASCO is located even further nasally. If this is the case, the difference in ASCO area between our report and previous reports will be even larger, necessitating future multiracial studies to further elucidate the role of ASCO enlargement in myopic eyes.

Posterior pole scleral thinning and deformation is known to occur histologically in highly myopic eyes,[44] and scleral changes such as posterior staphyloma are strongly associated with pathologic AXL elongation.[45] Our data imply that a mild scleral stretching and deformation caused by AXL elongation can already be observed in healthy myopic eyes with no apparent peripapillary scleral deformation on routine ophthalmic examination.

CpRNFLT has long been reported to become thinner with longer AXL.[46] However, when using a non-telecentric optical system such as in the case with the Topcon SS-OCT, the measurement circle under which cpRNFLT is measured is enlarged in eyes with longer AXL when magnification error correction is not performed.[47] If the total volume of RNFL can be assumed to be uniform within the scan area, the measured cpRNFLT will become thinner as the measurement circle diameter increases in eyes with longer AXL, which leads to the negative correlation between AXL and cpRNFLT reported in the magnification-uncorrected studies (Supplemental Figure S2).[46]

Later studies have estimated the magnification-corrected cpRNFLT from cpRNFLT values measured on the magnification uncorrected measurement circle, assuming that all RNFL

pass through both the uncorrected and corrected measurement circles and that the cross-sectional area under both circles are the same.[46] However, the linear relationship between the measurement circle diameter and RNFLT differs among ONH sectors,[48] and a uniform estimation may not be optimal. Hence, an evaluation of the relationship of cpRNFLT with AXL conducted with cpRNFLT measured on the corrected measurement circle position rather than the estimated cpRNFLT will be expected to be beneficial.

Our current results using cpRNFLT from AXL magnification-corrected measurement circle position demonstrated a positive association with longer AXL. Sector analysis of our data set (data not shown) revealed that only the temporal cpRNFLT is positively associated with AXL in accordance with previous reports using estimated magnification corrected cpRNFLT.[49, 50] One possible reason for a thicker cpRNFLT associated with longer AXL may be the temporally deviated cpRNFL distribution observed in highly myopic eyes.[51] The fact that MRW, which uses the BMO as a reference, was not significantly associated with AXL in our study suggests that MRW would be a more stable parameter to quantify peripapillary nerve fiber layer thickness in myopic eyes.

One limitation of this study is that we excluded eyes with hyperopia (SE >1 D) and may have overlooked hyperopic eyes with moderately elongated AXL. However, the incidence of myopia-like ONHs in hyperopic eyes is rare, and our AXL range of 22.2 to 27.4 mm should be enough to analyze the effect of AXL on the ONH structures of healthy myopic eyes.

Another limitation is the use of the BMO plane as a reference for measurement of LC depth. LC depth based on the BMO plane is known to be affected by age and choroidal thickness.[10] To manage this problem, we corrected for both effects of age and cpChT in our analysis to estimate the effect of LC depth referenced by the BMO plane on AXL.

Lastly, although the magnification correction method we used is considered to be the most accurate among the currently available methods, it may not be flawless and further research on the relationship between cpRNFLT and AXL may be necessary.

In conclusion, our study revealed that a greater misalignment between BMO and ASCO planes, which resulted in a more oblique choroidal border tissue configuration, a thinner choroid, a more posteriorly bowed peripapillary sclera configuration, and a larger ASCO area are associated with longer AXL in healthy myopic eyes. These findings are a foundation for future investigations to elucidate glaucoma-specific ONH changes that occur in glaucomatous myopic eyes.

Supplementary Material

Refer to Web version on PubMed Central for supplementary material.

Funding/Support:

Hitomi Saito was funded by Topcon and Japan Society for the Promotion of Science (project number: 20K18368); Atsuya Miki was funded by Council for Science, Technology and Innovation (CSTI) and the Cross-ministerial Strategic Innovation Promotion Program (SIP) “Innovative AI Hospital System”; Christopher Kai Shun Leung was funded by Topcon; Tae-Woo Kim was funded by Topcon; Linda Zangwill was funded by National Eye Institute (EY027510) and Topcon; and Robert Weinreb was funded by Topcon Corporation.

Financial Disclosure:

Hitomi Saito receives honoraria from Carl Zeiss Meditec, Topcon, Senju, Otsuka, Santen, Kowa, Novartis, Abbvie, and Viatris. Makoto Araie receives consultancy fees from Pfizer, Santen, Topcon, Senju, Aerie, and Kowa; honoraria from Pfizer, Senju, and Kowa; and licensing fees from GSTK-DiscAnalysis. Hiroshi Murata receives royalties from Kowa and Beeline. Tsutomu Kikawa is an employee of Topcon. Kazuhisa Sugiyama receives honoraria from Santen, Otsuka, Senju, Kowa, Novartis, Viatris, Bayers, and Inami Company. Tomomi Higashide receives honoraria from Bayer, HOYA, Kowa, Nitto Medic, Novartis, Otsuka, Santen, Senju, and Viatris. Atsuya Miki receives honoraria from Alcon, Ellex, Kowa, Menicon, Nitten, Nitto Medic, Otsuka, Rohto, SEED, Senju, and Viatris and consultancy fees from Santen. Aiko Iwase has a patent with Topcon and receives honoraria from Carl Zeiss Meditec, CREWT Medical Systems, Heidelberg Engineering, Santen, Senju, Otsuka, and Novartis and consultancy fees from Santen. Goji Tomita receives honoraria from Senju and Viatris. Toru Nakazawa receives grants and honoraria from Topcon Corp, Nidek, and Senju. Kyoko Ohno-Matsui receives consultancy fees from Santen and CooperVision. Makoto Aihara receives honoraria from Santen, Alcon, Pfizer, Otsuka, HOYA, TOMEY, CREWT Medical systems, Carl Zeiss Meditec, Senju, Novartis, Kowa, Johnson & Johnson, Glaukos, Iridex, and Canon; grants from Santen, Alcon, Pfizer, Otsuka, Johnson & Johnson, TOMEY, CREWT medical systems, Senju, Novartis, Kowa, Wakamoto, Glaukos, Ono, and Sato; consultancy fees from Santen, Alcon, Kowa, Wakamoto, Glaukos, Astellas, Senju, Pfizer, Otsuka, HOYA, and IRIDEX; and is on the advisory boards of Santen, HOYA, Senju, and Kowa. Christopher Kai Shun Leung receives licensing fees from Carl Zeiss Meditec; honoraria from Topcon and Santen; is on the advisory boards of Santen and Janssen; and receives equipment loan from Carl Zeiss Meditec and Heidelberg Engineering. Linda Zangwill receives grants from Heidelberg Engineering and Carl Zeiss Meditec; licensing fees from Carl Zeiss Meditec; consultancy fees from Abbvie and Digital Diagnostics; and received research instruments from Topcon, Optovue, Heidelberg Engineering, and Carl Zeiss Meditec. Robert Weinreb receives grants from National Eye Institute and Bausch & Lomb; licensing fees from Carl Zeiss Meditec; consultancy fees from Aerie Pharmaceuticals, Alcon, Allergan, Amydis, Equinox, Eyenovia, Iantrek, Implandata, IOPtic, Nicox, and Topcon; has patent with Toromedes; is on the advisory boards of Iantrek, Impandata, Amydid, and Eyenovia; is the chief editor of *International Glaucoma Review*; owns stock in Equonox, Eyenovia, Iantrek, Implandata, and IOPtic; and received research instruments from Heidelberg Engineering, Topcon, Carl Zeiss Meditec, Optovue, and Centervue. All authors attest that they meet the current ICMJE criteria for authorship.

REFERENCES

1. Holden BA, Fricke TR, Wilson DA, et al. Global prevalence of myopia and high myopia and temporal trends from 2000 through 2050. Ophthalmology. 2016;123(5):1036–1042. doi:10.1016/j.ophtha.2016.01.006. [PubMed: 26875007]
2. Haarman AEG, Enthoven CA, Tideman JWL, Tedja MS, Verhoeven VJM, Klaver CCW. The complications of myopia: a review and meta-analysis. Invest Ophthalmol Vis Sci. 2020;61(4):49. doi:10.1167/iovs.61.4.49.
3. Suzuki Y, Iwase A, Araie M, et al. Risk factors for open-angle glaucoma in a Japanese population: the Tajimi Study. Ophthalmology. 2006;113(9):1613–1617. doi:10.1016/j.ophtha.2006.03.059. [PubMed: 16828504]
4. Wang Y, Xu L, Zhang L, Yang H, Ma Y, Jonas JB. Optic disc size in a population based study in northern China: the Beijing Eye Study. Br J Ophthalmol. 2006;90(3):353–356. doi:10.1136/bjo.2005.081521. [PubMed: 16488961]
5. Tay E, Seah SK, Chan SP, et al. Optic disk ovality as an index of tilt and its relationship to myopia and perimetry. Am J Ophthalmol. 2005;139(2):247–252. doi:10.1016/j.ajo.2004.08.076. [PubMed: 15733984]
6. Kim M, Kim TW, Weinreb RN, Lee EJ. Differentiation of parapapillary atrophy using spectral-domain optical coherence tomography. Ophthalmology. 2013;120(9):1790–1797. doi:10.1016/j.ophtha.2013.02.011. [PubMed: 23672970]
7. Jonas JB, Jonas SB, Jonas RA, et al. Parapapillary atrophy: histological gamma zone and delta zone. PLoS One. 2012;7(10):e47237. doi:10.1371/journal.pone.0047237.
8. Kim YW, Lee EJ, Kim TW, Kim M, Kim H. Microstructure of β-zone parapapillary atrophy and rate of retinal nerve fiber layer thinning in primary open-angle glaucoma. Ophthalmology. 2014;121(7):1341–1349. doi:10.1016/j.ophtha.2014.01.008. [PubMed: 24565742]
9. Vianna JR, Malik R, Danthurebandara VM, et al. Beta and gamma peripapillary atrophy in myopic eyes with and without glaucoma. Invest Opthalmol Vis Sci. 2016;57(7):3103. doi:10.1167/iovs.16-19646.

10. Luo H, Yang H, Gardiner SK, et al. . Factors influencing central lamina cribrosa depth: a multicenter study. Invest Ophthalmol Vis Sci. 2018;59(6):2357–2370. doi:10.1167/iovs.17-23456. [PubMed: 29847642]
11. Ohno-Matsui K, Shimada N, Yasuzumi K, et al. Long-term development of significant visual field defects in highly myopic eyes. Am J Ophthalmol. 2011;152(2) 256–265.e1. doi:10.1016/j.ajo.2011.01.052. [PubMed: 21664594]
12. Ding X, Chang RT, Guo X, et al. Visual field defect classification in the Zhongshan Ophthalmic Center-Brien Holden Vision Institute High Myopia Registry Study. Br J Ophthalmol. 2016;100(12):1697–1702. doi:10.1136/bjophthalmol-2015-307942. [PubMed: 27033693]
13. Chang RT, Singh K. Myopia and glaucoma: diagnostic and therapeutic challenges. Curr Opin Ophthalmol. 2013;24(2):96–101. doi:10.1097/ICU.0b013e32835cef31. [PubMed: 23542349]
14. Sawada A, Tomidokoro A, Araie M, Iwase A, Yamamoto T. Refractive errors in an elderly Japanese population: the Tajimi study. Ophthalmology. 2008;115(2) 363–370.e3. doi:10.1016/j.ophtha.2007.03.075. [PubMed: 18243904]
15. Wong TY, Foster PJ, Hee J, et al. Prevalence and risk factors for refractive errors in adult Chinese in Singapore. Invest Ophthalmol Vis Sci. 2000;41(9):2486–2494. [PubMed: 10937558]
16. Tanito M, Nitta K, Katai M, et al. Differentiation of glaucomatous optic discs with different appearances using optic disc topography parameters: the Glaucoma Stereo Analysis Study. PLoS One. 2017;12(2):e0169858. doi:10.1371/journal.pone.0169858.
17. Potsaid B, Baumann B, Huang D, et al. Ultrahigh speed 1050nm swept source/Fourier domain OCT retinal and anterior segment imaging at 100,000 to 400,000 axial scans per second. Opt Express. 2010;18(19):20029–20048. doi:10.1364/oe.18.020029. [PubMed: 20940894]
18. Lavinsky F, Lavinsky D. Novel perspectives on swept-source optical coherence tomography. Int J Retina Vitreous. 2016;2:25. doi:10.1186/s40942-016-0050-y. [PubMed: 27847643]
19. Girard MJ, Tun TA, Husain R, et al. Lamina cribrosa visibility using optical coherence tomography: comparison of devices and effects of image enhancement techniques. Invest Ophthalmol Vis Sci. 2015;56(2):865–874. doi:10.1167/iovs.14-14903. [PubMed: 25593025]
20. Park HY, Shin HY, Park CK. Imaging the posterior segment of the eye using swept-source optical coherence tomography in myopic glaucoma eyes: comparison with enhanced-depth imaging. Am J Ophthalmol. 2014;157(3):550–557. doi:10.1016/j.ajo.2013.11.008. [PubMed: 24239773]
21. Sung MS, Heo MY, Heo H, Park SW. Bruch's membrane opening enlargement and its implication on the myopic optic nerve head. Sci Rep. 2019;9(1). doi:10.1038/s41598-019-55926-w.
22. Hong S, Yang H, Gardiner SK, et al. OCT-detected optic nerve head neural canal direction, obliqueness, and minimum cross-sectional area in healthy eyes. Am J Ophthalmol. 2019;208:185–205. doi:10.1016/j.ajo.2019.05.009. [PubMed: 31095953]
23. Jiang R, Wang YX, Wei WB, Xu L, Jonas JB. Peripapillary choroidal thickness in adult Chinese: the Beijing Eye Study. Invest Opthalmol Vis Sci. 2015;56(6):4045. doi:10.1167/iovs.15-16521.
24. Araie M, Iwase A, Sugiyama K, et al. Determinants and characteristics of Bruch's membrane opening and Bruch's membrane opening-minimum rim width in a normal Japanese population. Invest Ophthalmol Vis Sci. 2017;58(10):4106–4113. doi:10.1167/iovs.17-22057. [PubMed: 28828482]
25. Jeoung JW, Yang H, Gardiner S, et al. Optical coherence tomography optic nerve head morphology in myopia I: implications of anterior scleral canal opening versus Bruch membrane opening offset. Am J Ophthalmol. 2020;218:105–119. doi:10.1016/j.ajo.2020.05.015. [PubMed: 32445702]
26. Rezapour J, Tran AQ, Bowd C, et al. Comparison of optic disc ovality index and rotation angle measurements in myopic eyes using photography and OCT based techniques. Front Med (Lausanne). 2022;9:872658. doi:10.3389/fmed.2022.872658.
27. Harper AR, Summers JA. The dynamic sclera: extracellular matrix remodeling in normal ocular growth and myopia development. Exp Eye Res. 2015;133:100–111. doi:10.1016/j.exer.2014.07.015. [PubMed: 25819458]
28. Hodapp E, Parrish RK 2nd, Anderson DR. Clinical Decisions in Glaucoma. CV Mosby Co; 1993.
29. How AC, Tan GS, Chan YH, et al. Population prevalence of tilted and torted optic discs among an adult Chinese population in Singapore: the Tanjong Pagar Study. Arch Ophthalmol. 2009;127(7):894–899. doi:10.1001/archophthalmol.2009.134. [PubMed: 19597111]

30. Littmann H. Determining the true size of an object on the fundus of the living eye. Zur Bestimmung der wahren Grösse eines Objektes auf dem Hintergrund eines lebenden Auges. Klin Monbl Augenheilkd. 1988;192(1):66–67. doi:10.1055/s-2008-1050076. [PubMed: 3352190]

31. Han JC, Han SH, Park DY, Lee EJ, Kee C. Clinical course and risk factors for visual field progression in normal-tension glaucoma with myopia without glaucoma medications. Am J Ophthalmol. 2020;209:77–87. doi:10.1016/j.ajo.2019.08.023. [PubMed: 31493404]

32. Kim M, Choung HK, Lee KM, Oh S, Kim SH. Longitudinal changes of optic nerve head and peripapillary structure during childhood myopia progression on OCT: Boramae Myopia Cohort Study Report 1. Ophthalmology. 2018;125(8):1215–1223. doi:10.1016/j.ophtha.2018.01.026. [PubMed: 29550000]

33. Dai Y, Jonas JB, Huang H, Wang M, Sun X. Microstructure of parapapillary atrophy: beta zone and gamma zone. Invest Ophthalmol Vis Sci. 2013;54(3):2013–2018. doi:10.1167/iovs.12-11255. [PubMed: 23462744]

34. Sung MS, Heo H, Park SW. Microstructure of parapapillary atrophy is associated with parapapillary microvasculature in myopic eyes. Am J Ophthalmol. 2018;192:157–168. doi:10.1016/j.ajo.2018.05.022. [PubMed: 29859144]

35. Lee KM, Choung HK, Kim M, Oh S, Kim SH. Change of β-zone parapapillary atrophy during axial elongation: Boramae Myopia Cohort Study Report 3. Invest Ophthalmol Vis Sci. 2018;59(10):4020–4030. doi:10.1167/iovs.18-24775. [PubMed: 30098190]

36. Thakku SG, Tham YC, Baskaran M, et al. A global shape index to characterize anterior lamina cribrosa morphology and its determinants in healthy Indian eyes. Invest Ophthalmol Vis Sci. 2015;56(6):3604–3614. doi:10.1167/iovs.15-16707. [PubMed: 26047047]

37. Tun TA, Wang X, Baskaran M, et al. Variation of peripapillary scleral shape with age. Invest Ophthalmol Vis Sci. 2019;60(10):3275–3282. doi:10.1167/iovs.19-26777. [PubMed: 31369672]

38. Wang X, Tun TA, Nongpiur ME, et al. Peripapillary sclera exhibits a v-shaped configuration that is more pronounced in glaucoma eyes. Br J Ophthalmol. 2022;106(4):491–496. doi:10.1136/bjophthalmol-2020-317900. [PubMed: 33334817]

39. Farrar DE. Multicollinearity in regression analysis: the problem revisited. Rev Econ Stat. 1967;49(1):92–107. doi:10.2307/1937887.

40. Hirooka K, Fujiwara A, Shiragami C, Baba T, Shiraga F. Relationship between progression of visual field damage and choroidal thickness in eyes with normal-tension glaucoma. Clin Exp Ophthalmol. 2012;40(6):576–582. doi:10.1111/j.1442-9071.2012.02762.x. [PubMed: 22300430]

41. Rezapour J, Bowd C, Dohleman J, et al. The influence of axial myopia on optic disc characteristics of glaucoma eyes. Sci Rep. 2021;11(1):8854. doi:10.1038/s41598-021-88406-1. [PubMed: 33893383]

42. Wang YX, Yang H, Luo H, et al. Peripapillary scleral bowing increases with age and is inversely associated with peripapillary choroidal thickness in healthy eyes. Am J Ophthalmol. 2020;217:91–103. doi:10.1016/j.ajo.2020.03.050. [PubMed: 32298653]

43. Yang H, Luo H, Gardiner SK, et al. Factors influencing optical coherence tomography peripapillary choroidal thickness: a multicenter study. Invest Opthalmol Vis Sci. 2019;60(2):795. doi:10.1167/iovs.18-25407.

44. Vurgese S, Panda-Jonas S, Jonas JB. Scleral thickness in human eyes. PLoS One. 2012;7(1):e29692. doi:10.1371/journal.pone.0029692.

45. Ohno-Matsui K. Pathologic myopia. Asia Pac J Ophthalmol (Phila). 2016;5(6):415–423. doi:10.1097/apo.0000000000000230. [PubMed: 27898445]

46. Kang SH, Hong SW, Im SK, Lee SH, Ahn MD. Effect of myopia on the thickness of the retinal nerve fiber layer measured by Cirrus HD optical coherence tomography. Invest Ophthalmol Vis Sci. 2010;51(8):4075–4083. doi:10.1167/iovs.09-4737. [PubMed: 20237247]

47. Garway-Heath DF, Rudnicka AR, Lowe T, Foster PJ, Fitzk FW, Hitchings RA. Measurement of optic disc size: equivalence of methods to correct for ocular magnification. Br J Ophthalmol. 1998;82(6):643–649. doi:10.1136/bjo.82.6.643. [PubMed: 9797665]

48. Gabriele ML, Ishikawa H, Wollstein G, et al. Peripapillary nerve fiber layer thickness profile determined with high speed, ultrahigh resolution optical coherence tomography high-density

scanning. Invest Ophthalmol Vis Sci. 2007;48(7):3154–3160. doi:10.1167/iovs.06-1416. [PubMed: 17591885]

49. Ueda K, Kanamori A, Akashi A, Tomioka M, Kawaka Y, Nakamura M. Effects of axial length and age on circumpapillary retinal nerve fiber layer and inner macular parameters measured by 3 types of SD-OCT instruments. J Glaucoma. 2016;25(4):383–389. doi:10.1097/ijg.0000000000000216. [PubMed: 25580890]
50. Savini G, Barboni P, Parisi V, Carbonelli M. The influence of axial length on retinal nerve fibre layer thickness and optic-disc size measurements by spectral-domain OCT. Br J Ophthalmol. 2012;96(1):57–61. doi:10.1136/bjo.2010.196782. [PubMed: 21349942]
51. Hong SW, Ahn MD, Kang SH, Im SK. Analysis of peripapillary retinal nerve fiber distribution in normal young adults. Invest Ophthalmol Vis Sci. 2010;51(7):3515–3523. doi:10.1167/iovs.09-4888. [PubMed: 20164448]

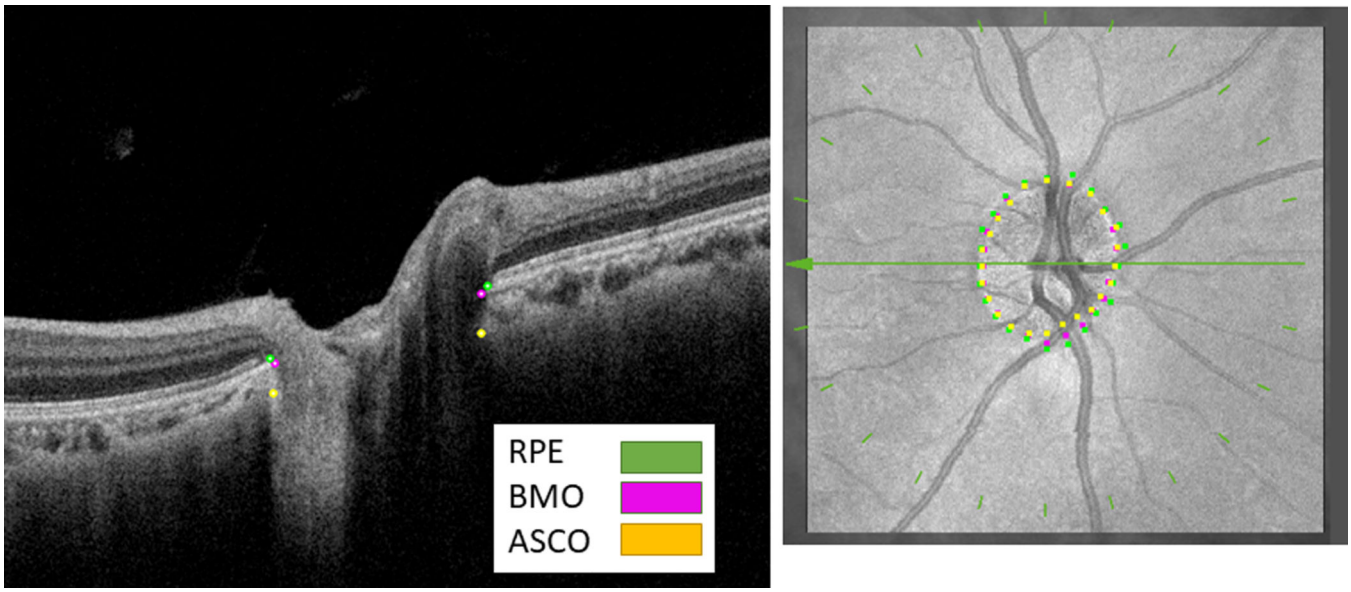

FIGURE 1.

Optic nerve head (ONH) segmentation determination on optical coherence tomography B-scans. Retinal pigment epithelium (RPE) edges (green dots), Bruch membrane opening (BMO) (pink dots), anterior scleral canal opening (ASCO) (yellow dots) were determined manually on 12 BMO-centered radial scans reconstructed from ONH raster scans. Contours of the RPE, BMO, and ASCO are overlayed on the infrared image on the right.

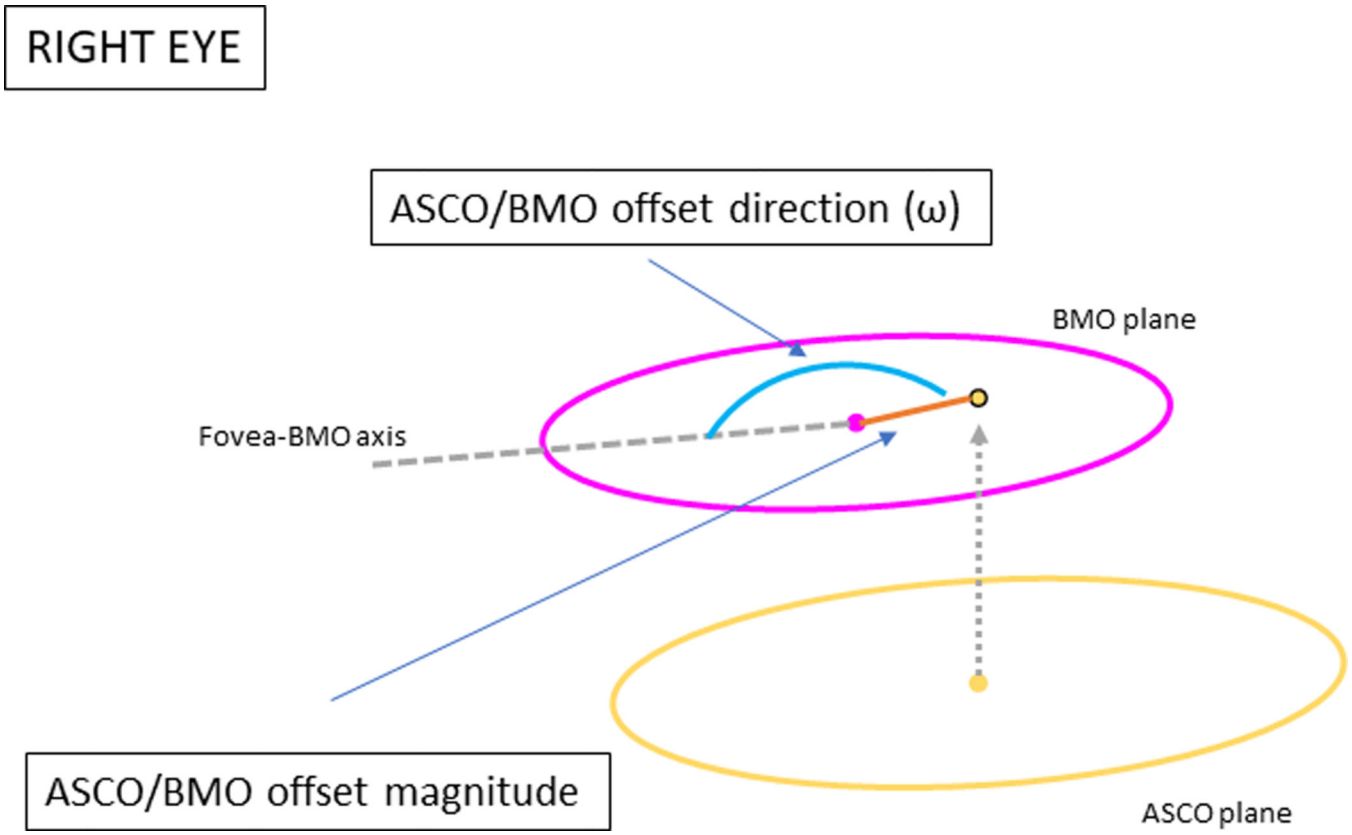

FIGURE 2.

Parameters defining the misalignment between Bruch membrane opening (BMO) and anterior scleral canal opening (ASCO). ASCO-BMO offset magnitude is the distance between the BMO centroid (pink dot) and ASCO centroid projected on the BMO plane (yellow dot with black outline). ASCO-BMO offset direction (ω) is the angle between fovea-BMO axis (gray dotted line) and ASCO/BMO centroid vector projected on the BMO plane (orange line).

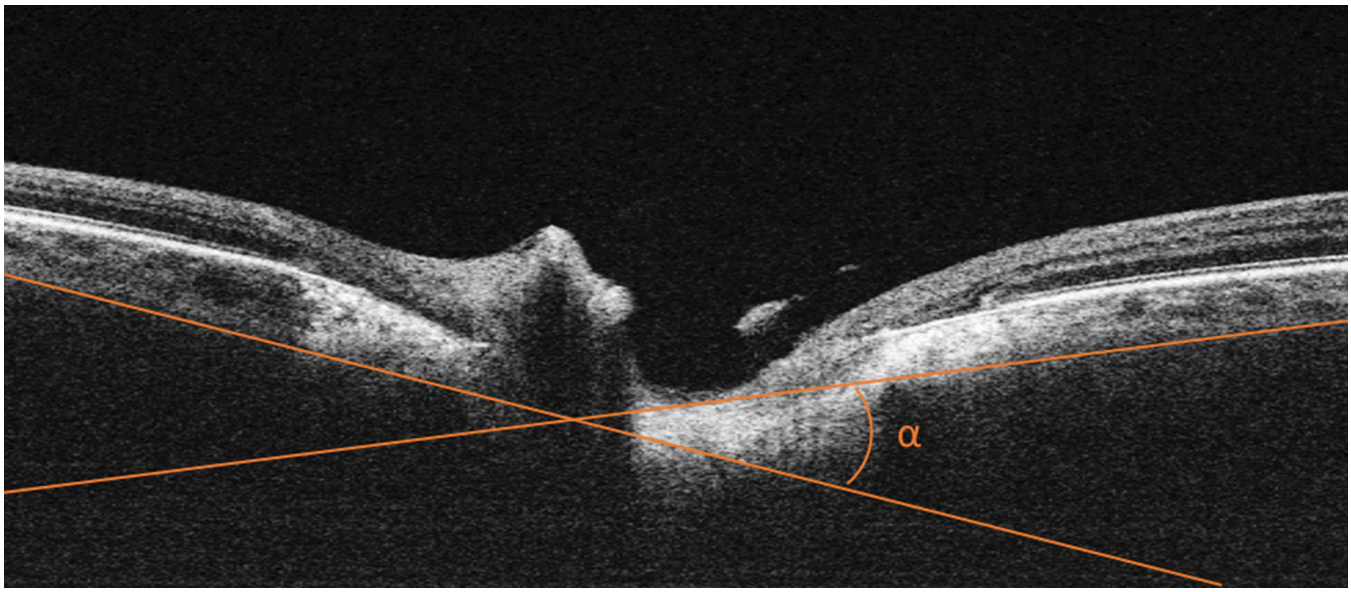

FIGURE 3.

Illustration of measurement of peripapillary scleral (PPS) angle. PPS angle (α) is defined as the angle between 2 lines parallel to the anterior scleral boundaries on a single horizontal B-scan in the nasal-temporal direction. A larger angle represents a more posteriorly bowed V-shaped PPS configuration.

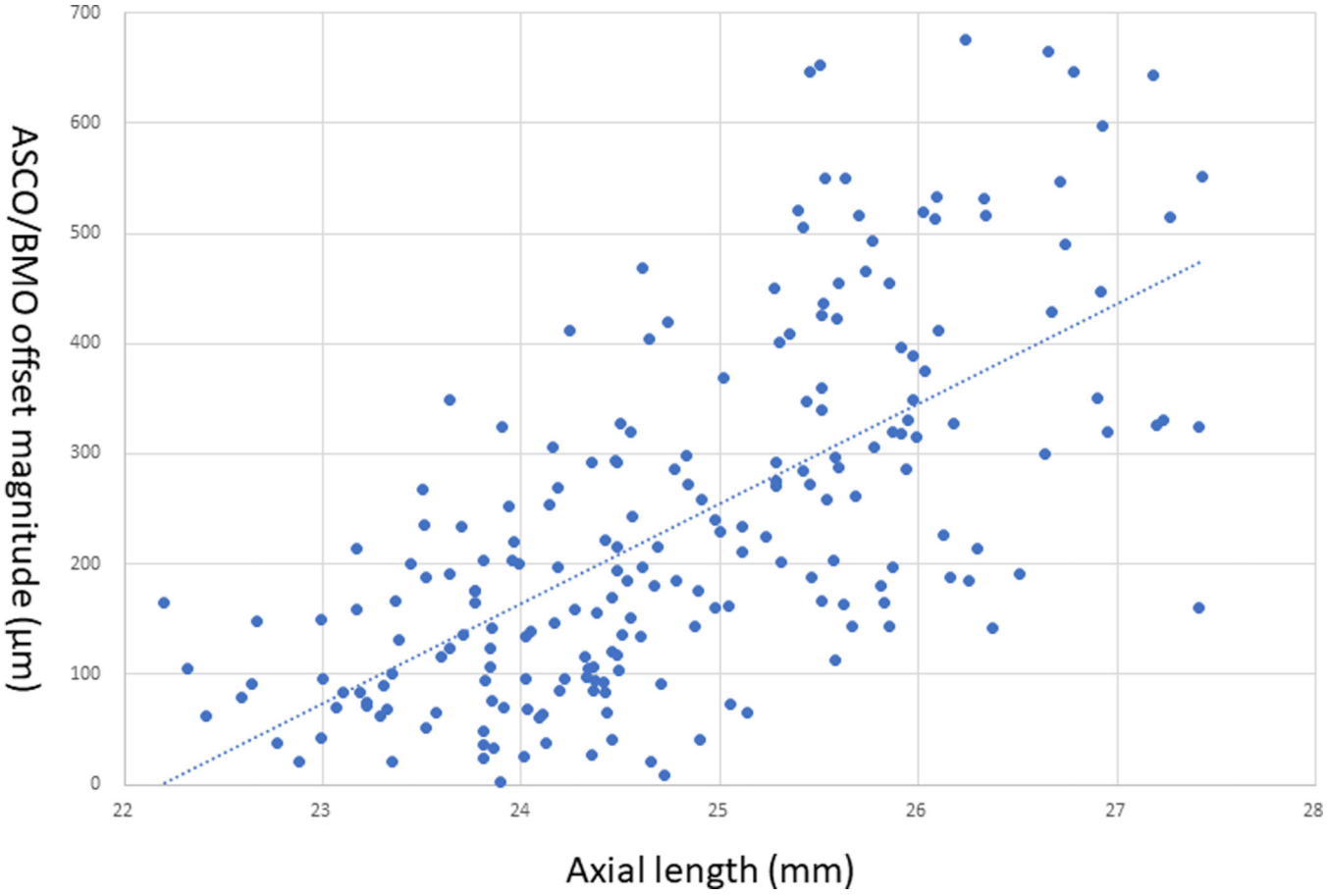

FIGURE 4.
Scattergram of axial length and ASCO-BMO offset magnitude.

Table 1.

Baseline characteristics

	211 eyes of 140 subjects
sex	M: 65 F: 75
R/L	R: 108 L: 103
Age	46.7±10.1 (30–71)
SE (diopter)	−3.09±2.41 (−9.13~+1.00)
AXL (mm)	24.79±1.15 (22.20~27.43)
MD (dB)	−0.22±1.14 (−3.48~2.29)
BMO area (mm^2)	2.17±0.54
BMO ovality	1.11±0.07
ASCO area (mm^2)	2.82±0.58
ASCO ovality	1.15±0.11
ASCO/BMO offset magnitude (μm)	236.8±158.9
ASCO/BMO offset direction (°)	162.8±45.1
Area of peri-neural canal RPE atrophy (mm^2)	0.75±0.56
Area of externally oblique choroidal border tissues (mm^2)	0.25±0.33
LC depth (μm)	427.0±98.4
LC-Global shape index	−0.78±0.22
Peripapillary Scleral angle (°)	6.43±4.19
Average MRW (μm)	292.6±51.0
cpRNFLT (μm)	108.5±6.0
cpChT (μm)	137.7±55.3

* values shown as average±standard deviation; () range

M=male; F=female; R=right; L=left; SE=spherical equivalence; AXL: axial length; MD: mean deviation; BMO=Bruch's membrane opening; ASCO=anterior scleral canal opening; PPA=peripapillary atrophy; LC=lamina cribrosa; MRW=minimum rim width; cpRNFLT=circumpapillary retinal nerve fiber layer thickness; cpChT=circumpapillary choroidal thickness.

Table 2.

Best fit linear mixed models with axial length as response variables.

		Standardized regression coefficient	Non-standardized regression coefficient	Standard Error	p-value*
Best fit model including ASCO-BMO offset magnitude	**ASCO/BMO offset magnitude**	**0.318**	**0.002**	**0.000**	**<0.0001**
	cpChT	**−0.221**	**−0.004**	**0.001**	**<0.0001**
	Peripaillary Scleral angle	**0.210**	**0.05**	**0.011**	**<0.0001**
	cpRNFLT	**0.156**	**0.017**	**0.005**	**0.008**
	MRW	0.102	0.002	0.000	0.72
	LC-GSI	0.043	−0.198	0.122	0.88
	ASCO ovality	0.042	0.381	0.233	0.88
	BMO ovality	0.037	0.536	0.395	0.96
Best fit model including area of externally oblique choroidal border tissues	Area of externally oblique choroidal border tissues	**0.288**	**0.861**	**0.182**	**<0.0001**
	ASCO area	**0.228**	**0.391**	**0.114**	**0.007**
	cpChT	**−0.221**	**−0.004**	**0.001**	**0.0007**
	cpRNFLT	**0.146**	**0.016**	**0.006**	**0.04**
	BMO area	0.250	−0.359	0.156	0.05
	MRW	0.102	0.002	0.001	0.52
	LC-GSI	0.043	−0.197	0.126	0.85

ASCO=anterior scleral canal opening; BMO=Bruch's membrane opening; cpChT=circumpapillary choroidal thickness; cpRNFLT=circumpapillary retinal nerve fiber layer thickness; LC-GSI=lamina cribrosa global shape index; MRW=minimum rim width;

*p-values after Bonferroni's correction by the number of included explanatory variables.